NUMERICAL ANALYSIS OF WIND INDUCED PRESSURE LOADS ON AN INTEGRATED ROOF-BASED PHOTOVOLTAIC SYSTEM

Marco Raciti Castelli [(a)], Sergio Toniato [(b)], Ernesto Benini [(c)]

[(a)] Department of Mechanical Engineering – University of Padua
Via Venezia, 1 – 35131 Padova, Italy
[(b)] ESPE S.r.l.
Via Cappello, 12/A – 35010 San Pietro in Gu (PD), Italy
[(c)] Department of Mechanical Engineering – University of Padua
Via Venezia, 1 – 35131 Padova, Italy

[(a)] marco.raciticastelli@unipd.it, [(b)] stoniato@espe.it, [(c)] ernesto.benini@unipd.it

ABSTRACT

Wind loads on the roof of a civil structure inside an industrial area still represent a great challenge for structural engineers. The quantitative amounts of force and pressure coefficients depend on the shape, size and orientation of the building and on its interaction with the surrounding environment.

The static loads due to wind pressure on a 5 deg pitched roof-based integrated photovoltaic system have been estimated by means of a 2D numerical simulation of the flow field around the T&T building in Valdagno (Italy). A constant wind velocity profile, based on the maximum reference wind speed in the building site (peak gust speed worked out for 50 years return period) and on the local roughness coefficient, has been simulated.

The distribution of wind-induced loads as a function of the panel row position and the amplitude of the recirculation region downstream the building have been determined, allowing a numerical quantification of the effect of the building geometry on the pressure loads on top of the roof.

Keywords: CFD, wind, building, roof

1. INTRODUCTION AND BACKGROUND

Due to the growing demand for renewable energy sources, the manufacturing of solar cells and photovoltaic arrays has shown a considerable advancement in recent years [1]. As of 2010, solar photovoltaic generated electricity in more than 100 countries and, while yet comprising a tiny fraction of the 4.8 TW total global power-generating capacity from all sources, is the fastest growing power-generation technology in the world [2]. However, as pointed out by Cosoiu et al. [3], the structure of the photovoltaic (PV) panel is rather flexible, continuous and fragile, sustained only by a thin framework. These features make it easily damageable by high winds and, in order to prevent such events, wind engineering experimental tests and numerical simulations are demanded if a more optimized and cheaper solution for a solar panel framework is required.

As focused by Krishna et al. [4], wind causes a random time-dependent load, which can be considered as a mean plus a fluctuating component. Strictly speaking, all civil structures experience dynamic oscillations due to the fluctuating component (gustiness) of wind, however, in short rigid structures, such oscillations are insignificant and the buildings can therefore be satisfactorily treated as being subjected to an equivalent static pressure. This approach is taken by most Codes and Standards. However, the response of a civil structure to high wind pressure depends not only on the geographical location and proximity of other obstructions to airflow, but also on the characteristics of the structure itself. As a matter of fact, most buildings present “bluff forms” to the wind, making it difficult to ascertain the wind forces accurately. Thus, the problem of bluff-body aerodynamics remains largely in the empirical/descriptive realm of knowledge. Furthermore, the flow patterns (and hence the wind pressure/forces) change with the Reynolds number, making the direct application of wind tunnel test results to real structures quite difficult [5]. Nevertheless, the limitations in accurate aerodynamic databases can be overcome by using advanced Computational Fluid Dynamics (CFD) codes, which can outflank the lack of experimental data thanks to their inherent ability to determine the aerodynamic components of actions through the integration of the Navier-Stokes equations. Performing CFD calculations can provide knowledge about the flow-field around the building in all its details, such as velocities, pressure, etc. Moreover, all types of useful graphical presentations, such as flow lines, contour lines

and iso-lines are readily available. As suggested by Jensen et al. [6], this stage can be considered as if an accurate wind-tunnel study or an elaborate full-scale measurement campaign had been conducted. The numerical prediction of wind loads on buildings as a branch of Computational Wind Engineering (CWE) was well introduced by Franke [7], who described the different simulation approaches with their corresponding basic equations and the necessary turbulence models.

Wind loading on solar panels depends on three basic elements: the wind speed, the height of the panel above the roof, and the relative location of the panel on the roof: in fact, pressure loads will depend on the location of the module on the roof (with different net pressure coefficients applied for those near the roof edge), whether the roof has a parapet and whether the PV support structure is open or fully clad. Moreover, as pointed by Dalgliesh [8], roof angle strongly affects the flow around a low-rise building: as a direct consequence, the flow field over a 5 deg pitched roof building is dominated by flow separation.

Hoxey et al. [9] performed both full-scale experiments and CFD calculations in order to investigate the main geometric parameters that affect wind loads on low-rise buildings. The study focused on the use of numerical simulations so as to assess the sensitivity of wind loads to changes in height, span and roof pitch.

More recently, Dagnew et al. [10] performed several comparison between CFD and experimental analysis, in order to assess the potential use of numerical wind load predictions approaches for practical use. The work revealed the suitability of CFD tools for preliminary assessments and detail explanation of complex building aerodynamic characteristics.

In order to develop a preliminary procedure to be used as a guidance in selecting the appropriate grid configuration and corresponding turbulence model for the prediction of the flow field over a two-dimensional roof architecture dominated by flow separation, Raciti Castelli et al. [11] recently tested the capability of several turbulence models to predict the separation that occurs in the upstream sector of the roof and the extension of the relative recirculation region for different vertical longitudinal positions, respectively from the upstream leading edge to the downstream bottom edge of a reference model building. Also spatial node distribution was investigated, in order to determine the best compromise between numerical prediction accuracy and computational effort. The numerical code proved *Standard k-ε* turbulence model to be quite accurate in predicting the flow-field features, especially after the recirculation region in the upstream portion of the model roof. On the basis of this preliminary study, in the present work the flow field over a 5 deg pitched roof-based integrated photovoltaic system was numerically investigated, in order to determine the distribution of wind loads as a function of the panel row position on the roof and the amplitude of the recirculation region downstream the building.

2. THE CASE STUDY

The proposed numerical simulations were based upon the T&T building in Valdagno (Northern Italy). Figure 1 shows an aerial view of the building site, located inside an industrial area placed on a wind plain close to a low hilly area.

Figure 1: Aerial view of the T&T building site (the analyzed building is evidenced by the red rectangle)

Figure 2: Top view of the T&T building double 5 deg gabled roof enclosed by a continuous brick fence

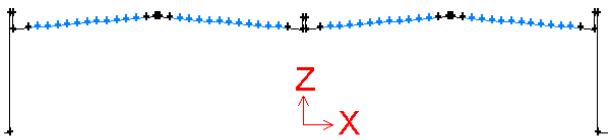

Figure 3: Main vertical section of the T&T building

Table 1: Main dimensions of the T&T building

$H_{building}$ [m]	12
$L_{building}$ [m]	60
α [deg]	5
$H_{lateral\ fence}$ [m]	1.6
$H_{central\ fence}$ [m]	1.05

As can be seen from Figures 2 and 3, the T&T building is a rectangular structure characterized by a double 5 deg gabled roof enclosed by a continuous lateral brick fence 1.6 m high and a central one 1.05 m high. Table 1 summarizes the main geometrical features of the analyzed building. A total number of 52 rows of PV panels are to be deployed on the top of the roof, 13 for each roof pitch.

3. MODEL GEOMETRY

In order to simulate a wind flow directed orthogonally into the face of the PV panels, a 2D simulation was performed. Table 2 summarizes the main geometrical features of the computational domain, which is also reproduced in Figure 4.

Table 2: Main geometrical features of the computational domain

L_{domain} [m]	2400
H_{domain} [m]	600
L_1 [m]	600

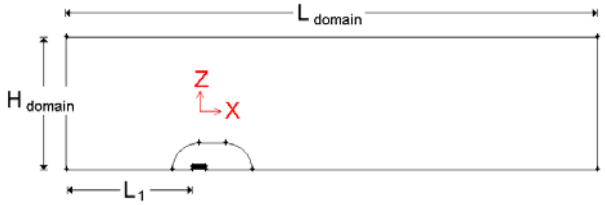

Figure 4: Main dimensions of the computational domain

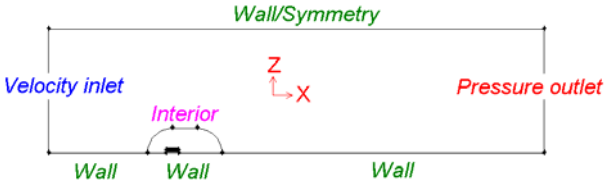

Figure 5: Boundary conditions of the computational model

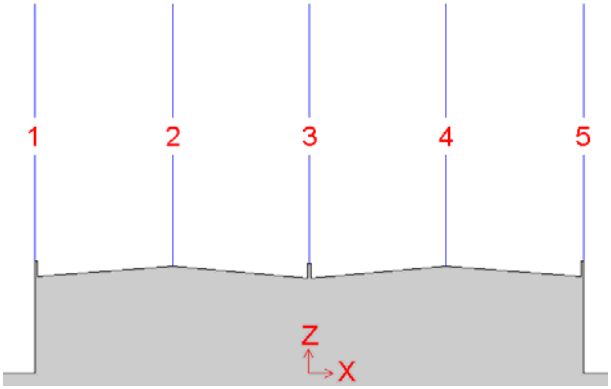

Figure 6: Displacement of the five reference positions (along the roof length) that were used for x-component mean velocity computation

The numerical model boundary conditions are represented in Figure 5. As suggested by Raciti Castelli et al. [11] both "*Wall*" and "*Symmetry*" boundary conditions were tested for the upper portion of the computational domain, and their influence on the numerical results proved completely negligible.

Table 3: Normalized x-coordinates of the five reference positions with respect to the model building length (the origin of the coordinate reference system is located at the model building center, as evidenced from Figure 3)

Reference position No.	$x_{ref,norm}$
1	-0.50
2	-0.25
3	0.00
4	0.25
5	0.50

The vertical profiles of the x-component mean velocity were computed at five reference positions along the roof length. Figure 6 shows the displacement of the reference positions, whose normalized x-coordinates with respect to the model building length, defined as:

$$x_{ref,norm} = x_{ref}/L_{building} \quad (1)$$

are reported in Table 3.

4. SPATIAL DOMAIN DISCRETIZATION

An isotropic unstructured mesh was created around the model building. Considering their features of flexibility and adaption capability, unstructured meshes are in fact very easy to obtain, for complex geometries, too, and often represent the "first attempt" in order to get a quick response from the CFD in engineering work.

The same spatial grid resolution suggested by Raciti Castelli et al. [11] was adopted for the present calculations. In Table 4 the characteristic data of the adopted grid architecture are reported, as a function of the normalized grid resolution on the building, defined as:

$$Res_{building} = \Delta g_{building}/H_{building} \quad (2)$$

and as a function of the normalized grid resolution on outer computational domain, defined as:

$$Res_{domain} = \Delta g_{domain}/H_{domain} \quad (3)$$

Table 4: Characteristic data of the adopted grid architecture

$Res_{building}$ [-]	Growth factor [-]	Res_{domain} [-]
0.025	1.25	0.07

For further details upon the validation procedure and the reliability of the adopted numerical settings (as

far as grid resolution and turbulence model are concerned), see [11].

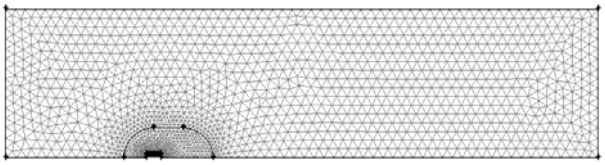

Figure 7: Main geometrical features of the adopted grid resolution

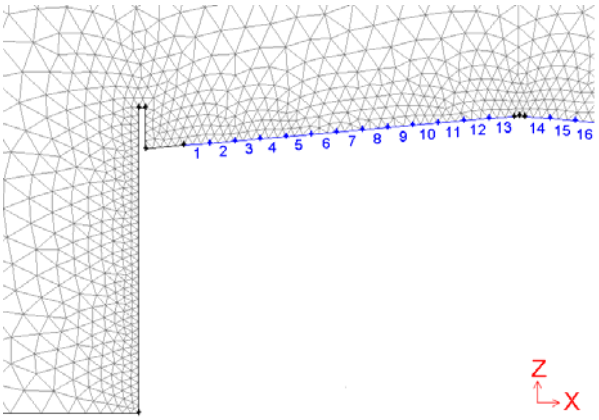

Figure 8: Main geometrical features of the adopted grid refinement near the building and numbering of the PV rows on the top of the roof, respectively from 1 to 52 starting from the building upwind leading edge (on the left)

Figures 7 and 8 show the main features of the adopted grid. Figure 8 shows also some of the numbered panel rows on the top of the roof, respectively numbered from 1 to 52 starting from the building upwind leading edge.

Table 5: Main coefficients adopted for the calculation of the maximum reference wind speed on the T&T building site, according to [12]

$v_{b,0}$ [m/s]	25
a_0 [m]	1000
a_s [m]	60
v_b [m/s]	25
c_t [-]	1
k_r [-]	0.22
z_0 [m]	0.30
z_{min} [m]	8
$c_e(H_{building})$ [-]	1.91
$v_{b,max}$ [m/s]	34.5

5. DETERMINATION OF INLET WIND VELOCITY PROFILES

A constant velocity profile, based on the maximum reference wind speed in the building site (peak gust speed worked out for 50 years return period) was computed. After determining from [12] the values of $v_{b,0}$, a_0, c_t, k_r, z_0 and z_{min} for the building site, the reference wind speed was determined as:

$$v_b = v_{b,0} \quad (4)$$

being:

$$a_s \leq a_0 \quad (5)$$

and the coefficient of exposure for the building site was determined as:

$$c_e(H_{building}) = k_r^2 \, c_t \, ln(H_{building}/z_0)[7+c_t \, ln(H_{building}/z_0)] \quad (6)$$

being:

$$H_{building} \geq z_{min} \quad (7)$$

The maximum reference wind speed for the building site was eventually determined as:

$$v_{b,max} = [v_b^2 \, c_e(H_{building})]^{0.5} \quad (8)$$

Table 5 summarizes the main coefficients adopted for the calculation of the maximum reference wind speed.

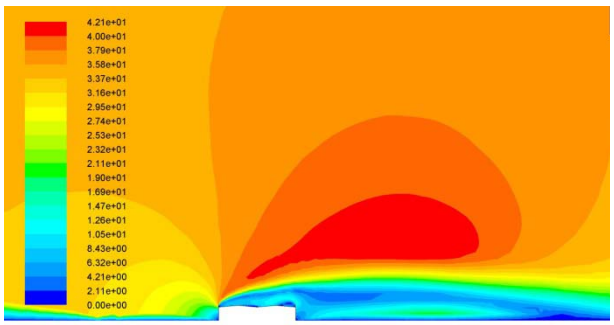

Figure 9: Contours of absolute velocity magnitude [m/s] on the surroundings of the T&T site

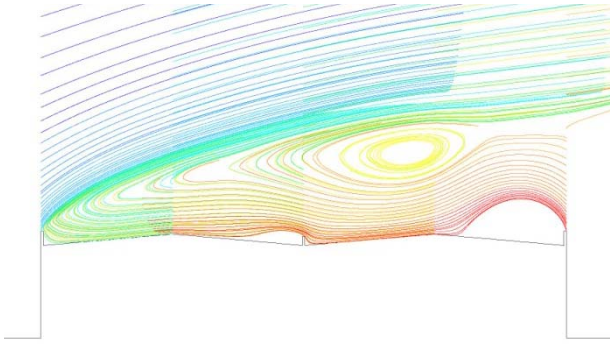

Figure 10: Visualization of absolute pathlines, colored by particle variables and starting from the five reference positions. A huge separation bubble associated to the vertical recirculation zone on the top of the building is visible

6. TURBULENCE MODEL AND CONVERGENCE CRITERIA

Simulations were performed using the commercial RANS solver ANSYS FLUENT®, which implements 2-D Reynolds-averaged Navier-Stokes equations using a finite volume-finite element based solver. A segregated solver, implicit formulation, was chosen for unsteady flow computation. The fluid was assumed to be incompressible, being the maximum fluid velocity on the order of 42 m/s. *Standard k-ε* model was used for turbulent calculations, as suggested from [11].

As a global convergence criterion, residuals were set to 10^{-5}. The simulations, performed on a 8 processor, 2.33 GHz clock frequency computer, required a total CPU time of about 3 hours.

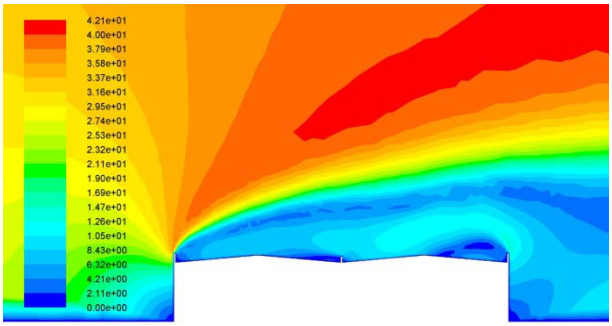

Figure 11: Contours of absolute velocity magnitude [m/s] close to the T&T building

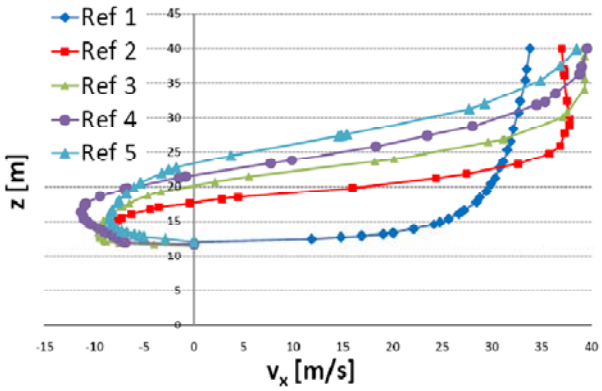

Figure 12: Computed x-velocity profiles for the five reference positions

7. RESULTS AND DISCUSSION

Figure 9 shows the contours of absolute velocity magnitude on the surroundings of the T&T site. As can be clearly seen, velocities close to the structure result much higher (up to 42.1 m/s) with respect to the constant (34.5 m/s) inlet velocity profile.

A recirculation zone on top of the roof and downstream of the building can be seen from Figure 10, representing the velocity pathlines colored by particle variables and also from Figure 11, showing the contours of absolute velocity magnitude close to the T&T building.

Figure 12 shows the computed x-velocity profiles for the five reference positions on the top of the T&T building. Flow separation is clearly visible, as well as the recirculation zone. It can also be noticed that, while reference position No. 1 presents no recirculation, the amount of reverse flow increases starting from reference position No. 2 and shows a peak in correspondence of reference position No. 4 (violet line).

Figures from 13 to 15 show the horizontal, vertical and resultant forces for unit length on solar panel rows along the T&T building as a function of the PV panel row number.

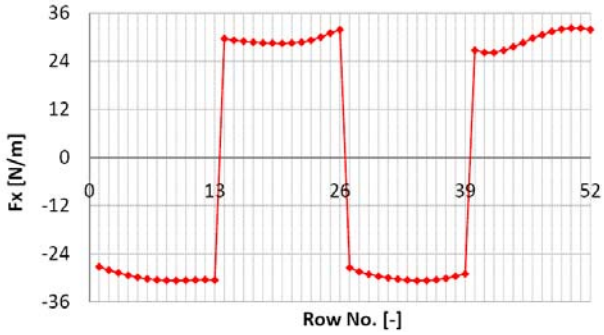

Figure 13: Horizontal force on PV panel rows for unit length along the T&T building

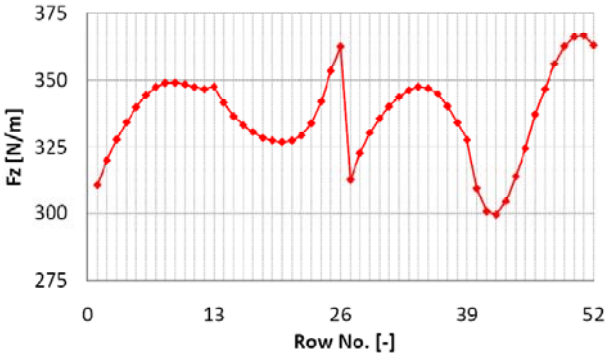

Figure 14: Vertical force on PV panel rows for unit length along the T&T building.

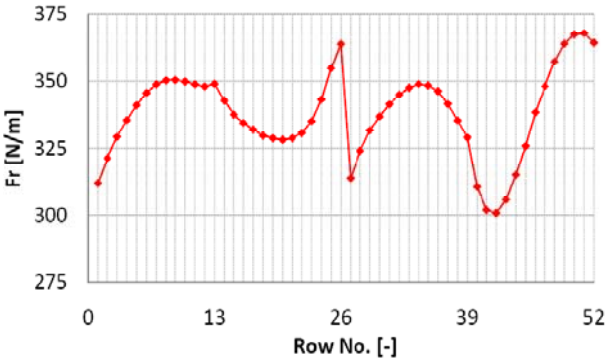

Figure 15: Resultant (total) force on PV panel rows for unit length along the T&T building

It can be noticed that, thanks to the continuous lateral brick fence on the whole perimeter of the roof, no downward force is registered on the PV panel rows. On the contrary, all panels are subjected to upwards thrusts, due to the low pressure in the recirculation zone

on the top of the building, as can be seen from Figures 14 and 16, showing the contours of static pressure close to the T&T site. It can be argued that the described phenomenon is related to a vertical suction occurring in the whole roof, due to a dramatic decrease of static pressure, as a consequence of the large separation bubble on the top of the building.

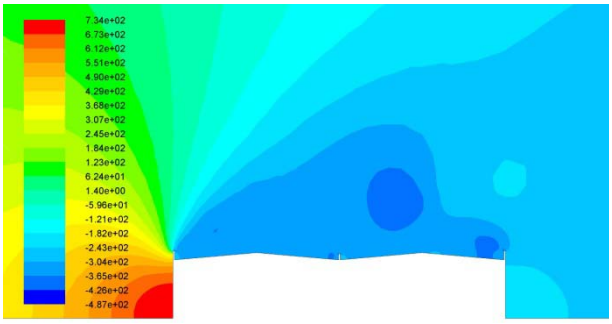

Figure 16: Contours of static pressure [Pa] close to the T&T building

As can be seen, the horizontal force is negligible if compared to the vertical one, being the latter nearly 10 times higher. A discontinuity in the horizontal force per unit length can be observed in correspondence of the top/bottom of the roof pitches. Also the vertical force presents a discontinuity in correspondence of the center of the building.

A periodicity in the vertical force distribution is registered, each period corresponding to a double-pitched portion of the roof. Moreover, the influence of the central brick fence on wind induced pressure loads appears to be negligible.

8. CONCLUSIONS AND FUTURE WORKS

A numerical model for the evaluation of wind induced pressure loads on a 5 deg pitched roof-based integrated PV system was presented. A constant wind velocity profile, based on the maximum reference wind speed in the building site (peak gust speed worked out for 50 years return period) and on the local roughness coefficient, was simulated.

A large recirculation zone was registered, causing reverse flow in the vertical x-velocity profiles on the top of the building.

It was proved that, thanks to a continuous lateral brick fence on the whole perimeter of the roof, no downward force is registered on the PV panel rows. On the contrary, all panels resulted subjected to upward thrusts, due to the low pressure in the recirculation zone on the top of the building. The influence of the central brick fence on wind induced pressure loads resulted negligible.

Further 3D work should be performed in order to investigate the influence of a lateral wind flow on the PV panel rows.

ACKNOWLEDGMENTS

The present work was performed in cooperation with E.S.P.E. S.r.l., San Pietro in Gu (Italy) in order to develop a numerical model for the prediction of the turbulent flow field around the T&T building, Valdagno (Italy).

NOMENCLATURE

a_0 [m]	reference height above sea level for T&T building site
a_s [m]	height above sea level for T&T building site
$c_e(H_{building})$ [-]	coefficient of exposure for T&T building site and height
c_t [-]	coefficient of topography for T&T building site and height
F_x [N]	horizontal force on PV panel rows for unit length
F_r [N]	resultant (total) force on PV panel rows for unit length
F_z [N]	vertical force on PV panel rows for unit length
$H_{building}$ [m]	building height
$H_{lateral\ fence}$ [m]	lateral brick fence height
$H_{central\ fence}$ [m]	central brick fence height
H_{domain} [m]	computational domain height
k_r [-]	reference roughness coefficient at T&T building site
L_1 [m]	distance between computational domain inlet condition and building
$L_{building}$ [m]	building length
L_{domain} [m]	computational domain length
Res_{domain} [-]	normalized grid resolution on outer computational domain
$Res_{building}$ [-]	normalized grid resolution on the building
$v_{b,0}$ [m/s]	basic wind speed at T&T building site
v_b [m/s]	basic wind speed at T&T building site and height above sea level
$v_{b,max}$ [m/s]	maximum reference wind speed at T&T building site
$v_m(z)$ [m/s]	average wind velocity profile at T&T building site
v_x [m/s]	x-component of wind velocity on top of the T&T building
x_{ref} [m]	x-coordinate of the reference position for x-component mean velocity computation
$x_{ref,norm}$ [-]	normalized x-coordinate of the reference position for x-component mean velocity computation
z_0 [m]	reference height of roughness coefficient for T&T building site
z_{min} [m]	minimum reference height of roughness coefficient for T&T building site
α [deg]	gabled roof inclination with respect to the horizontal
Δg_{domain} [m]	grid resolution on outer computational domain

$\Delta g_{building}$ [m] grid resolution on the building

REFERENCES

[1] Lacey, S., April 26, 2011. *Creating Investor Certainty in Large-Scale Solar*, Inside Renewable Energy podcast.

[2] September 2010. *Renewables 2010 Global Status Report*, REN21.

[3] Cosoiu, B., Damian, A., Damian, R. M., Degeratu, M., June 11-13, 2008. *Numerical and Experimental Investigation of Wind Induced Pressures on a Photovoltaic Solar Panel*, 4th IASME/WSEAS International Conference on ENERGY, ENVIRONMENT, ECOSYSTEMS and SUSTAINABLE DEVELOPMENTS (EEESD'08), Algrave, Portugal.

[4] Krishna, P., Kumar, K., Bhandari, N. M. *IS:875 (Part3): Wind Loads on Buildings and Structures – Proposed Draft & Commentary*, Document No. IITK-GSDMA-Wind02-V5.0 and IITK-GSDMA-Wind04-V3.0.

[5] Bhandari, N. M., Krishna, P., Kumar, K., Gupta, A. *An Explanatory Handbook on Proposed IS 875 (Part3) – Wind Loads on Buildings and Structures*, Document No. IITK-GSDMA-Wind06-V3.0.

[6] Jensen, A. G., Franke, J., Hirsch, C., Schatzmann, M., Stathopoulos, T., Wisse, J., Wright, N. G., 2004. CFD Techniques – *Computational Wind Engineering*, Proceedings of the International Conference on Urban Wind Engineering and Building Aerodynamics – Impact of Wind and Storm on City Life and Built Environment – Working Group 2, COST Action C14, Von Karman Institute, Rode-Saint-Genèse (Belgium).

[7] Franke, J., *Wind Effects on Buildings and Design of Wind-Sensitive Structures*, CISM International Centre for Mechanical Sciences, 2007, Vol. 493, pp. 67-103.

[8] Dalgliesh, W. A., January 1981. *Wind Loads on Low Buildings*, Division of Building Research, National Research Council of Canada, Ottawa.

[9] Hoxey, R. P., Robertson, A. P., Basara, B., Younis, B. A., *Geometric Parameters that Affect Wind Loads on Low-Rise Buildings: Full-Scale and CFD Experiments*, Journal of Wind Engineering and Industrial Aerodynamics, Vol. 50, Dec. 1993, pp. 243-252.

[10] Dagnew, A. K., Bitsuamalk, G. T., Merrick, R., *Computational Evaluation of Wind Pressures on Tall Buildings*, 11th Americas Conference on Wind Engineering, San Juan, Puerto Rico, June 22-26, 2009.

[11] Raciti Castelli, M., Castelli, A., Benini, E., July 27-29, 2011. *Modeling Strategy and Numerical Validation of the Turbulent Flow over a two-Dimensional Flat Roof*, ICCFD 2011, Paris (France).

[12] DM 14/01/2008 – *Norme tecniche per le costruzioni*, issued on the Italian "Gazzetta Ufficiale" on February 4, 2008.

AUTHORS BIOGRAPHY

Marco Raciti Castelli is Research Associate at the Department of Mechanical Engineering of the University of Padua and Fluid Dynamic Specialist at ESPE S.r.l.

Sergio Toniato is Executive and Design Manager at ESPE S.r.l.

Ernesto Benini is Associate Professor at the Department of Mechanical Engineering of the University of Padua.